Mixing of dust aerosols into a mesoscale convective system: Generation, filtering and possible feedbacks on ice anvils

Pierre Tulet, K. Crahan-Kaku, Maud Leriche, Benjamin Aouizerats, Suzanne Crumeyrolle

Mixing of dust aerosols into a mesoscale convective system. Generation, filtering and possible feedbacks on ice anvils.☆

P. Tulet*

Meteo-France, CNRM/GAME 42 Gaspard Coriolis 31057 Toulouse, France
LACy, Université de La Réunion, 15 Av René Cassin, 97715 Saint-Denis

K. Crahan-Kaku

Meteo-France, CNRM/GAME 42 Gaspard Coriolis 31057 Toulouse, France

M. Leriche

Laboratoire d'Aérologie/CNRS, Université de Toulouse 14 av Ed Belin 31400 Toulouse, France

B. Aouizerats

Meteo-France, CNRM/GAME 42 Gaspard Coriolis 31057 Toulouse, France

S. Crumeyrolle

Meteo-France, CNRM/GAME 42 Gaspard Coriolis 31057 Toulouse, France

Abstract

During the second Specific Observing Period (SOP) of the African Monsoon Multidisplinary Analyses (AMMA) campaign, several intense Mesoscale Con-

*Corresponding author
Email addresses: pierre.tulet@meteo.fr (P. Tulet), katie@atmos.washington.edu (K. Crahan-Kaku), maud.leriche@aero.obs-mip.fr (M. Leriche), benjamin.aouizerats@cnrm.meteo.fr (B. Aouizerats), s.crumeyrolle@opgc.univ-bpclermont.fr (S. Crumeyrolle)

vective Systems (MCS) developed over Niger. An examination of a particular convective storm simulated with a mesoscale model near Banizoumbou, Niger, on 1 July, 2006, shows that this MCS generates a strong emission of dust particles at the leading edge of its density current. A fraction of these dust aerosols are uplifted by the convective core of the system and redistributed by aqueous processes. Aerosol impaction scavenging is the main process by which particles are deposited within the mesoscale convective system. However, small particles (smaller than $1\mu m$) that are not efficiently scavenged, are able to reach the upper troposphere at a concentration of 6 particles per cm^3. This suggests that deep convection over semi-arid regions is able to create its own ice nuclei in high concentrations. This leads to the question: can deep convection over semi-arid regions affect particular ice properties such as ice anvil extension or induce possible feedbacks of dust on precipitation through ice sedimentation?
Key words: dust, aerosol scavenging, ice nuclei, gust front, Mesoscale Convective Systems

---

1. Introduction

Mineral dust contributes significantly to the global radiative budget calculations through absorption and scattering of longwave and shortwave radiation (Houghton et al., 2001), and its indirect effect on cloud microphysics (IPCC, 2007), (Twomey, 1959), (Albrech, 1989), (Sandu et al., 2008)). At a local level, high dust concentrations are shown to impact the vertical structures of storms (Lohmann and Diehl, 2006) and local energy budgets (Grini et al., 2006). The dust diameters have a large range in size, from below

0.2 to 40 μm, implying that different sink mechanisms need to be correctly modeled, such as sedimentation, wet and dry deposition. Dry deposition includes turbulent transfer to the surface and gravitational settling. Wet deposition includes nucleation scavenging and impaction scavenging, both involving complex microphysical interactions between aerosols and hydrometeors. Nucleation scavenging describes the activation of aerosols into cloud droplets and ice crystals and subsequent growth to precipitating hydrometeors. Impaction scavenging is the collection of the aerosols by cloud droplets, ice crystals and precipitating hydrometeors through Brownian motion, interception, inertial impaction, thermophosphoresis, diffusiophoresis, airflow turbulence and electrostatic attraction in and below the cloud layer (Andronache, 2003). Usually, impaction scavenging by iced hydrometeors are not considered in numerical models because of its low effect compared to collection by liquid particles. Theoretically, impaction scavenging is usually split into two processes: in-cloud impaction scavenging that treats the interactions between cloud droplets and raindrops with interstitial aerosol particles, and below cloud scavenging that concerns the collection of aerosol particles by falling raindrops below the cloud base. The relative importance of in-cloud scavenging processes (nucleation and impaction scavenging), also called washout, and below cloud scavenging, also called rainout, depends on meteorological conditions and on the properties of aerosol particles (size distribution and chemical composition) as well as on the stage of cloud development. Global models have estimated that wet deposition only accounts for 10% of the total dust loss globally (Tegen and Lacis, 1996; Ginoux et al., 2001). Locally, wet deposition can be expected to play a larger role in dust

removal processes, especially in areas of intense convection, as observed during the monsoon season in West Africa.

The data acquired in the framework of the 2006 African Monsoon Multidisciplinary Analyses (AMMA) field campaign (Redelsperger et al., 2006) provides an excellent opportunity to analyze the processes of dust generation and deposition associated with convection. Within semi-arid regions, the strong winds associated with gust fronts of Mesoscale Convective Systems (MCSs) generate dust and aerosol lofting. Some recent studies have detailed the dust formation in the leading edge of the density current observed in the intertropical discontinuity region (Flamant et al., 2007, 2009; Marsham et al., 2008). The dust generation associated with the 1 July, 2006 MCS (SOP 2 of the AMMA campaign) was modeled near the Niamey and Banizoumbu region (Niger) and compared to observations by Crumeyrolle et al. (2008). The present work is an extension of the Crumeyrolle et al. (2008) study with a special focus on the generation and the vertical transport of dust in the convective core of a MCS in relation to precipitation. In particular, several aspects of a MCS over a semi-arid region that can cause feedbacks of dust on ice in the upper troposphere are emphasized.

2. Model Description

2.1. General parameterizations

The MesoNH model has been jointly developed by the CNRM (Météo-France and Centre National de la Recherche Scientifique) and Laboratoire d'Aérologie (Centre National de la Recherche Scientifique and Université de

Toulouse) (Lafore et al., 1998). MesoNH simulates small scale atmospheric circulation (horizontal resolution of a few meters) to synoptic scale (horizontal resolution of several tens of kilometers) and can be run in a two-way nested mode involving up to 8 nesting stages. Parameterizations have been introduced for convection (Bechtold et al., 2001), cloud microphysics (Pinty and Jabouille, 1998; Cohard and Pinty, 2000), turbulence (Bougeault and Lacarrere, 1989), biosphere-atmosphere thermodynamic exchanges (ISBA) (Noilhan and Mahfouf, 1996), urban-atmosphere interactions (Masson, 2000), lightning processes (Barthe et al., 2005), gaseous chemistry (Suhre et al., 1998; Tulet et al., 2003) and aerosols chemistry (Tulet et al., 2006).

2.2. Mineral dust parameterization

Mineral dust emissions are parameterized following Grini et al. (2006). In this parameterization, the three lognormal modes are generated and transported by the ORILAM lognormal aerosol scheme (Tulet et al., 2005). Regarding emission processes, dust aerosols are mobilized using the Dust Entrainment and Deposition model (DEAD) (Zender et al., 2003) which calculates dust fluxes from wind friction speeds. The physical basis of the model is taken from Marticorena and Bergametti (1995) in which dust fluxes are calculated as a function of saltation and sandblasting processes. Here, the emission of dust aerosols is calculated directly from ISBA surface parameters, and then sent to the atmosphere consistently with the fluxes of momentum, energy and humidity. The initial dust size distribution contains three modes with median radii of 0.32, 1.73 and 4.33 μm and standard deviations of 1.7, 1.6 and 1.5, respectively as defined by Alfaro and Gomes (2001).

2.3. The ICE3 cloud microphysics scheme

The study uses the ICE3 cloud microphysics scheme described by Pinty and Jabouille (1998). This scheme follows the approach of Lin et al. (1983) in that a three-class ice parameterization is coupled to a Kessler's scheme for warm processes. It is a bulk single moment scheme that predicts the evolution of the mixing ratios of six water species (vapor, cloud droplets and raindrops, pristine ice, snow and graupel). Pristine ice crystal are here assumed to be plates. The precipitation of water drops and ice crystals is parameterized according to Caniaux et al. (1994). The size distribution of the hydrometeors is assumed to follow a generalized γ-law function in normalized form. Due to the use of a single moment bulk scheme, this study does not consider the cloud condensation nuclei and ice nuclei activation. There is no interaction between the dust particles and the microphysics within the model.

2.4. Impaction scavenging and aerosol-cloud interactions

The impaction scavenging of aerosols is calculated in MesoNH based upon first order principals. In- and below-cloud impaction scavenging by cloud droplets and raindrops uses a kinetic approach to calculate the aerosol mass transfer as:

$$\frac{dM_p}{dt} = -\Lambda_M M_p \tag{1}$$

where dMp/dt represents the aerosol dry mass transfer in the aqueous phase, M_p the aerosol dry mass and Λ_M the path normalized scavenging coefficient in s^{-1}. For impaction scavenging by cloud droplets, the main process to consider is the Brownian motion of dry aerosols and cloud droplets (Pruppacher and

Klett, 2000) leading to the normalized scavenging coefficient determined by the semi-empirical formulation as:

$$\Lambda_M M_p = \frac{1.35 LWC D_p}{r_{cloud}^2} \tag{2}$$

where LWC is the cloud liquid water content in $g.cm^{-3}$, D_p is the diffusivity of the particle in $m^2.s^{-1}$ and r_{cloud} the cloud droplet radius in m.

The impaction scavenging by raindrops depends mainly on Brownian motion, interception, and inertial impaction following a formula originally described by Slinn (1983):

$$\Lambda_M M_p = \frac{3}{2}\frac{E}{r_{rain}}.F_{rain} \tag{3}$$

where E is the collection efficiency fully described in Seinfeld and Pandis (1997); Tost et al. (2006), r_{rain} the radius of the rain droplets in mm and F_{rain} the effective precipitation flux in $kg.m^{-2}.s^{-1}$.

Within this impaction scavenging scheme, the efficiency is calculated for three types of collection. Small particles are collected efficiently by raindrops and cloud droplets through Brownian diffusion, but the collection efficiency decreases with increasing particle size. Inertial impaction by raindrops is important for large particles, with collection efficiencies approaching one for particles with diameter greater than 20 μm. Inside the cloud, impaction scavenging by cloud droplets is less efficient for particles with diameters from 0.2 to 2.0 μm. Indeed interception by raindrops is difficult since particles follow the streamlines of air around the falling droplets. The in-cloud mass aerosol tranfer into rain droplets by autoconversion and accretion processes have been introduced as described by Pinty and Jabouille (1998). The sedimentation of aerosol mass included in raindrops is solved using a time splitting

technique with an upstream differencing scheme of the vertical flux as:

$$P_{asr} = \frac{m_{aero}}{m_{rain}\rho}\frac{d}{dz}(V_r.\rho.r_{rain}) \quad (4)$$

where P_{asr} is the raindrops aerosol mass sedimentation rate, m_{aero} the aerosol mass included in raindrops in $kg.kg^{-1}$, m_{rain} the rain water mass in $kg.kg^{-1}$, ρ the air density and V_r the raindrop sedimentation velocity in $m.s^{-1}$.

As for the microphysical scheme, only mass transfer between aerosols and warm cloud processes have been considered here. As a consequence the model follows the aerosol mass of each lognormal mode during its evolution through the warm ICE3 processes. Indeed the aerosol scheme is limited to one moment (mass) during its warm processes exchange. This limitation involves two assumptions: (1) Mass transfer does not change the size distribution of the aerosol modes, and (2) the rerelease of aerosols into the air due to rain evaporation is proportional to the mass of water evaporated (Chin et al., 2000). As a consequence, the mean radii and standard deviation of the raindrops aerosol modes are identical to the dry aerosol size distribution, implying that neither coagulation nor chemical transformation occurred in the cloud droplets are considered in the model. The second assumption however, is likely to overestimate the release of aerosols due to evaporation as some evaporation of the rain results in smaller raindrops that still contain the aerosols.

2.5. Model configuration

The simulation begins at 00 UTC on June 29, 2006, and ends at 00 UTC on July 2, 2006. Three two-way nested domains are used. The large domain at 36 km resolution (3.1°S - 31.7°N; 25.64°W - 35.64°E) gives a

large scale synoptic view of west Africa. The first embedded domain (12 km resolution) is centered over northwest Nigeria and covers a large part of the AMMA campaign area (4.3°N - 17.6°N; 4.19°W - 16.24°E). The embedded smallest domain at 3 km resolution (11.80°S - 16.82°N; 0.10°W - 8.31°E) gives a fine scale view of Niger. For the two larger domains, the Bechtold et al. (2001) convection scheme is used, whereas deep convection is assumed to be explicitly resolved at 3 km resolution. Only the smallest domain is examined in this study. The vertical grid is composed of 60 stretched vertical levels reaching the altitude of 34,000 meters above ground level (m agl); 30 levels are located in the boundary layer between the surface and 2,000 m agl. Initialization and lateral boundary conditions of the large domain are taken from the ECMWF analysis.

Two types of simulations have been performed. The complete simulation (SCAV) uses the dust scavenging scheme whereas the NOSCAV simulation do not include wet deposition for dust. Because there is no connection of dusts with dynamics and microphysics, these two simulations give identical MCSs. Actually, the difference between these two simulations shows the impact of precipitation on the dust distribution.

3. Mesoscale convection and dust generation

This section focus on the vertical structure of a MCS observed and simulated east of Banizoumbou the 1^{st} of July at midnight. Figures 1.a, 1.c and 1.e display the MSG brightness temperature (at 10.8 μm) on 1 July 2006 at 18 UTC, 2 July at 00 UTC and 2 July at 02 UTC, respectively (Chaboureau and Pinty, 2006). The MSG satellite images show the passage of several con-

vective systems over the south-east of Niger: most of the MCSs are triggered at the eastern part of the simulated domain (Fig. 1.a) and propagate to the west over the Niamey and Banizoumbou region. The two most intense systems are observed north of and over Banizoumbou between 00 UTC and 02 UTC (Fig. 1.c and 1.e). The northern MCS is triggered 3° north-east of Banizoumbou (Fig. 1.a) and propagates to Niamey and Burkina Faso (Fig. 1.c and 1.e). The second system is triggered at 2.5° east of Banizoumbou (Fig. 1.a). It moves slowly (Fig. 1.c) and disappears over Banizoumbou (Fig. 1.e).

Figures 1.b, 1.d and 1.f give the cloud top height (dashed) and the instantaneous precipitation (isolines) simulated by MesoNH on 1 July 2006 at 16 UTC, 18 UTC and 20 UTC, respectively. As observed previously on the satellite images, some convective systems are simulated over the south-east of Niger where the two main systems have reached the Niamey region. The system north is triggered on 1 July 2006 at 16 UTC, at 1° north-east of Banizoumbou (Fig. 1.b). This difference in the initiation location will cause a 5 hours time lag in the passage of the systems over the Niamey and Banizoumbou region. However it evolves similarly to observations, except for passing a bit too south of Niamey (Fig. 1.c, 1.d, 1.e and 1.f). The southern system begins 2.5 ° east of Banizoumbou at the same location as observed on the MSG images, but one hour earlier than observed (Fig. 1.a and 1.b). Furthermore, its propagation is quite different from the observed MCS. At 20 UTC, the system is simulated 1° southeast of Banizoumbou (Fig.1.d) and instead of disappearing on Banizoumbou (Fig. 1.e), the system continues its propagating to the border of Burkina-Fasso (Fig. 1.f).

The overshoot of the modeled MCS reaches 19,000 m agl in the lower stratosphere and the top of the anvil is simulated at 16,000 m agl at the altitude of the tropopause. The area of detrainment is spread over a large area located at the tropopause. By comparison between the MSG images and the simulation, one can observe that differences exists in the location of triggering and in the stage of the cycle life. However, these differences should not strongly affect the focus of this article; the major features of these MCS are realistic enough and characteristic of convection systems over west Africa.

The instantaneous simulated precipitations (isolines) have been superimposed to the altitude of the cloud top (isolines on Fig. 1.b, 1.d and 1.f). The maximum of observed precipitation gives the cloud zone where the convection is strong. The cell simulated at the south-east of Banizoumbou at 20 UTC (Fig 1.d) is particularly active with the precipitation rate reaching 50 $mm.h^{-1}$ at the surface.

MCS downdrafts create a gust front where surface winds exceed 15 $m.s^{-1}$. This gust front can be seen on Figure 2 by surface winds vector divergence in the front of each MCS. The associated surface winds are greater than the wind speed threshold of 6.5 $m.s^{-1}$ for soil erosion determined by Chomette et al. (1999) over Sahelian-Saharian regions. However, around the MCSs, the surface winds are low (less that 5 $m.s^{-1}$) and they cannot produce dust emission (Fig. 2). As a consequence, only in the MCS gust front, winds are for the most part strong enough to move soil particles by saltation and generate high dust concentration at the surface as simulated by the model ahead and west of the MCS (Fig.2). More than 10,000 $\mu g.m^{-3}$ of dust are simulated at the surface east of Banizoumbou and 5,000 $\mu g.m^{-3}$ over Niamey. Three

others gust fronts with high dust concentration are simulated in the northern part of the domain. They are created by the small convective cells simulated at 19 UTC (not shown) and 20 UTC (Fig. 1.d). Note that the intense dust plume formed in this northern area, is mainly due to the soil characteristics and to the absence of any vegetation.

Simulation validation through observation data was detailed by Crumeyrolle et al. (2008): it was shown that the increase of the surface wind speed, the decrease of surface pressure and the measured precipitation at the arrival of the MCS are correctly reproduced over Niamey. In addition, the dust mass concentration profile in the lower troposphere simulated over the Niamey region before and after the MCS passage are closed to the ATR42 aircraft observations. The next section of the paper focuses on a particular cell which was simulated at the east of Banizoumbou (Fig.2). This cell is significant in the high concentration of dust contained in the gust front (about 3,000 $\mu g.m^{-3}$) and the associated precipitation rate is important (50 $mm.h^{-1}$). Furthermore, this cell generates considerable levels of detrainment in the upper troposphere as shown in Figure 1.d.

4. Dust formation and redistribution in the convective cloud

Figure 3 gives the vertical cross section of the total condensed water by the solid line delineated on the Figure 2 (the left corner of the cross section corresponds to the south west point of the solid line). The simulated vertical velocity reached 20 $m.s^{-1}$ between 9,000 m agl and 15,000 m agl, (black isolines of Fig. 3), that represents the convective core of the system. More than 2.5 $g.kg^{-1}$ of condensed water is simulated within this convective core.

Detrainment of the system is modeled at the tropopause located at 16,000 m agl. The convective overshoot reaches 19,000 m agl and transports to the lower stratosphere more than 1 $g.kg^{-1}$ of total condensed water. Above 6,000 m agl, rainfall appears with a maximum of 4 $g.kg^{-1}$ at 2,000 m agl under the convective core.

This intense precipitation (evaporation and drag of hydrometeors) plays an important role in the downdrafts and the cold pool formation at the surface. This cold pool is characterized by low potential temperature (298 K), 7 degrees lower than its environment and a negative buoyant air (Fig. 4.a). However, at the leading edge of the gust front identified by the surface winds convergence (streamlines in Figure 4.a), the vertical gradient of potential temperature is null between the surface and 2,000 m agl, showing that the air of this frontal region is mixed in this layer. Within the cold pool and the frontal zone, the turbulent kinetic energy modeled is greater than 2 $m^2.s^{-2}$ (shaded area on Figure 4.a). Indeed the air from the gust front is mixed by turbulence in the frontal zone and the winds convergence has forced the air to rise dynamically above the gust front.

Figure 4.b gives the vertical cross section of the dust concentration (SCAV simulation). On the right side of this Figure, the Sahelian boundary mixing layer appears with about 200 $\mu g.m^{-3}$ of dust. High surface winds associated with the gust front (more than 12 $m.s^{-1}$ at 10 m agl) generate sandblasting and a saltation flux of dust particles at the surface (Figure 4.b). Within the cold pool, 1,500 $\mu g.m^{-3}$ of dust is simulated in the complete simulation (SCAV) of Figure 4.b. At the leading edge of the gust front, dust is transported upward in the ascending current and entrained into the cloud.

Knippertz et al. (2009) have also found similar results where strong emission of dust have been engendered by density current associated to moist convection over the Atlas Mountains. This entrainment of dusty air in the cloud is also visible by the curvature of the streamlines of Figure 4.a. Precipitations (marked by the shaded area of Figure 4.b) scavenges most of the dust mass concentration entrained into the cloud. They also contributes to decreases significantly the dust concentration simulated in the cold pool: the maximum of rain mixing ratio at the surface (2 $g.kg^{-1}$) corresponds to a local minimum of dust concentration. Moreover, beyond this maximum, a second band of precipitation (1 $g.kg^{-1}$) corresponding to a cumulus simulated in front of the MCS, also contribute to limit the dust concentration at the east part of the gust front. Despite of these precipitations, in the SCAV simulation, 500 and 100 $\mu g.m^{-3}$ of these fresh particles produced in the gust front remains at 1,000 m agl and 3,000 m agl, respectively. Dust concentrations decreases to 30 $\mu g.m^{-3}$ at 6,000 m agl (not shown). Flamant et al. (2007) and BouKaram et al. (2008) showed that the frontal zones like the inter-tropical discontinuity are favorable to dust lifting through turbulence. At a more local scale and over desert, gust fronts associated to single convection cell, also generate dust particles and transport aerosols above the boundary layer.

Without any dust scavenging (NOSCAV simulation), the modeled dust concentration is much larger, reaching 3000 $\mu g.m^{-3}$ in the gust front (Fig. 5). Convection lifts more than 300 $\mu g.m^{-3}$, 100 $\mu g.m^{-3}$ and 50 $\mu g.m^{-3}$ of dust formed in the gust front to 5,000 m agl, 10,000 m agl, and 16,000 m agl, respectively. At the tropopause, these particles are detrained far from the convective core in the anvil.

Figure 6 shows the differences between the dust mass concentration of the two simulations NOSCAV and SCAV. In both simulations, the dynamics and cloud microphysics are the same. In-cloud, the differences of dust mass concentration between the two simulations (NOSCAV-SCAV) are on the same order of magnitude as the dust concentration simulated in the NOSCAV simulation, showing that the dust mass is close to zero in the cloud of the simulation SCAV. This implies that most of the dust mass concentration has been scavenged by raindrops. Indeed, with dust scavenging, less than 1500 $\mu g.m^{-3}$ of dust is modeled in the cold pool and as little as 15 $\mu g.m^{-3}$ is able to reach 8,000 m agl. Furthermore, some notable differences are modeled in the rain and cloud evaporation zones at the rear part of the MCS. Some of the dust particles collected by cloud droplets and raindrops are re-released in the SCAV simulation in the evaporative zones where the precipitation does not reach the surface. It results in more than 200 $\mu g.m^{-3}$ of dust mass near the surface due to precipitation evaporation. This can be observed behind the MCS and during the dissipation stage (Figure 6). Note that these released dust particles have likely enhanced hygroscopic properties caused by soluble materials within the monsoon flux coating the mineral dust (Levin et al., 1996; Crumeyrolle et al., 2008). Indeed, precipitations serve contradicting purposes: it washes out most of the dust mass in the gust front, but it play also a major role in the production of fresh dust.

5. Dust vertical distribution and aerosol size filtering

The profile of mass and number concentration for the three dust modes are plotted in Figure 7 along the cross section of Figure 6 indicated by the

vertical dashed line. Note that this profile corresponds to the convective region of the MCS except between 3,000 m agl and 8,000 m agl where the profile is at the boundary of the cloud which is indicated by a decrease in the plotted dust concentration. The vertical profile of the smaller mode with the median radius of 0.32 μm is the same for both SCAV and NOSCAV simulations (green solid and dashed lines are superimposed on Figure 7). It indicates that this mode is not affected by impaction scavening since these particles are two large to be collected by Brownian motion and too fine to have significant inertial velocities (i.e. collection by inertial impaction). The collection efficiency factor is less than 0.5 % for the smallest particles mode whereas for the two larger ones (with median radii of 1.73 μm and 4.33 μm) the efficiency factors are 30 and 99 % respectively. As a consequence, the majority of the dust concentration of the two larger modes has been scavenged and 99 % of the mass of the smallest mode is preserved and is able to be transported upward in the convective core. The vertical profile of Figure 7.a shows that the precipitation decreases the dust mass concentration above 2,000 m agl from 150 $\mu g.m^{-3}$ ($R_g = 1.73\ \mu m$ and $R_g = 4.33\ \mu m$) to 30 $\mu g.m^{-3}$ ($R_g = 1.73\ \mu m$) and 8 $\mu g.m^{-3}$ ($R_g = 4.33\ \mu m$). Between 3,000 m agl and 9,000 m agl, a local maximum of the two larger modes is observed in the SCAV simulation and corresponds to a local minimum of the NOSCAV simulation. As explained before, this area is at the boundary of the cloud and this local maximum corresponds to evaporated rain and cloud droplets that re-release some new dusts. In the upper troposphere above 15,000 m agl, the mass concentration from the SCAV simulation reaches respectively 6 $\mu g.m^{-3}$ ($R_g = 0.33\ \mu m$), 0.8 $\mu g.m^{-3}$ ($R_g = 1.73\ \mu m$) and 0.4 $\mu g.m^{-3}$ ($R_g = 4.33$

μm) whereas the total mass concentration modeled in the NOSCAV simulation is 50 $\mu g.m^{-3}$. Indeed, within the SCAV simulation the majority of the mass transported near the tropopause is due to the first mode, representing 80 % of the total mass, whereas this mode represents only 10 % of the total emitted mass.

Even though most of the aerosol mass has been scavenged, the number of small particles reaching higher altitudes still are significant within the SCAV simulation (Figure 7.b). The SCAV simulation shows that 20 particles per cm^3 have been transported to 7,000 m agl and more than 6 particles per cm^3 reach the tropopause (16,000 m agl). This represents 1 to 2 % of the number concentration modeled at the surface in the gust front whereas only 0.4 % of the mass concentration in the gust front reach the upper troposphere.

These results show that the MCS precipitations are two-fold. Firstly, rainfall (drag of hydrometeors and evaporation) is one of the main mechanism that generates downdrafts and causes the formation of a gust front. When convection is located over a dust source region, dust particles are formed in the cold pool, ahead of the precipitation zone, where the soil is dry enough. The size distribution of the emitted dust depends on the wind friction at the surface and thus is also influenced by surface conditions and by the intensity of downdrafts. That is as the emitted dust modes are strongly dependent on the energy of impaction during the sandblasting (Alfaro and Gomes, 2001): the stronger the surface wind, the greater the respective concentration of the smallest particles. A part of these fresh aerosols, which are located at the leading edge of the cold pool, can be entrained in the cloud updraft. Secondly, rainfall filters the size distribution of particles by preserving the first

mode and scavenging the two larger modes. Our model shows that a large number of small particles can be transported by convection. In this case study, more than 6 particles per cm^3 reached the tropopause.

6. Dust transport in the UTLS

On July, 2 at 00 UTC (Figure 1), the simulation shows that the upper level of the MCS detrainment is modeled at 16,000 m agl at the tropopause. At this altitude, more than 6 dust particles per cm^3 have been transported up to the convective core of each MCS (Fig. 8.a). High dust concentration up to 0.2 cm^{-3} are spreading over the main part of the south-west of Niger. The previously studied MCS gets the most intense plume dust concentration: more than 2 cm^{-3} of dust particles have been modeled on a surface exceeding 22,500 km^2. Figure 8.b shows that in the lower stratosphere (at 20,000 m agl) the overshoot of the most intense MCS can transport high concentration of dust particles (with maxima reaching over 0.1 cm^{-3}). As for water vapor, it is known that convection is an important source of aerosol in the lower stratosphere. For the first time, IN concentration was measured during the CRYSTAL-FACE campaign in Florida (Prenni et al., 2007) using a continuous flow diffusion chamber sampling residual particles remaining after evaporation of cloud particles initially collected by a counterflow virtual impactor. These measurements were made onboard the citation aircraft in anvil of convective clouds at altitudes between 8 and 11 km corresponding to the upper troposphere in Florida. In this study, the range of measured IN concentration is 0.001 to 1 cm^{-3} whereas it is 0.2 to 6 cm^{-3} in the simulated MCS in the upper troposphere over Africa. This suggests that the

order of magnitude of aerosol produced and transported by the MCS over African semi-arid regions are high and greater than over Florida (DeMott et al., 2003).

7. Conclusion

This study emphasizes several important aspects of dust emissions which can be formed in the gust front of a MCS over semi-arid region. In the simulations, this process models dust concentrations greater than 3000 $\mu g.m^{-3}$ at the surface. Without wet dust scavenging (NOSCAV), about 50 $\mu g.m^{-3}$ of dust is transported in the convective core and reaches the tropopause, whereas less than 1 $\mu g.m^{-3}$ is modeled in the complete simulation (SCAV). Indeed, precipitations filter the main part of the super-micronic dust mode and the sub-micronic mode (here at a median radius of 0.32 μm) is preserved. This mode represents 10 % of the emitted mass but 98 % of the aerosol number. A large number of dust particles reaches the tropopause, with a maximum of 6 particles per cm^3 at 16,000 m agl. This number concentration is several orders of magnitude greater than ice nuclei observed over Florida during the CRYSTAL-FACE campaign where there is no local dust emissions comparable from a semi-arid region. Considering that mineral dust can serve as good ice nuclei (Kanji and Abbatt, 2006; Richardson et al., 2007), the dust generated by convection may influence the ice number concentration near the tropopause. It is assumed that if high ice nuclei concentrations are able to significantly decrease the supersaturation in the section of cloud containing ice, we can expect that dust can play an important role in the type of ice crystals (Nelson, 2001). It is also possible that the modification of the size

and type of ice crystals can also affect the lifetime of anvils and impact the convective precipitation (Gilmore et al., 2004b) through the ice sedimentation velocity in the upper troposphere. Another study from Gilmore et al. (2004a) compared cloud resolving model simulations results using liquid-only and liquid and ice phase microphysics. They underlined the role of the ice phase in increasing precipitation production aloft and producing stronger downdrafts and greater low-level downward precipitation fluxes (and ground accumulations) compared to liquid-only simulations. In addition, the variation of ice-forming nuclei concentration leads to changes in hail sizes, which are known to have a great impact on the dynamic, thermodynamic and precipitation characteristics of the resulting storm (van den Heever and Cotton, 2004).

Some studies on the effects of dust on the masses of various ice species within the anvils of convective storms during CRYSTAL-FACE dedicated to the Florida convection have been perfomed by van den Heever et al. (2006) and Carrio et al. (2007). These studies used the mesoscale model RAMS, which includes simple a parameterization for connecting the concentration of CCN and IFN and the nucleated droplets and ice crystals. These studies have shown that IFN concentrations have a greater impact on updraft strength during the mature and dissipating storm stages.

Moreover, a recent study based on satellite and direct aircraft measurement during NAMMA (a part of AMMA operated by NASA) supports the hypothesis that Saharan dust may have led to invigoration of rain bands associated with tropical cyclogenesis near West African coastline (Jenkins et al., 2008). Another recent study (Min et al., 2009), that uses some multi-platform and

multi-sensor observations, shows that the consequences of dust on a particular MCS observed over the Gulf of Guinea were to shift the precipitation size spectrum from heavy rain to light rain. At this stage several questions arise on the particular properties of MCS formed over semi-arid regions: (1) Are anvil lifetimes and spatial dimensions affected by the dust aerosols generated by downdrafts? (2) Does a feedback exist between dust and precipitation by limitating the ice sedimentation in the upper troposphere? On the one hand observations alone cannot answer these questions due to the difficulties of de-aliasing the meteorological particularities of each MCS. On the other hand, mesoscale models need to improve their parameterization of ice microphysics processes to include a realistic scheme of ice activation before sensitivity studies on ice nuclei impacts can be performed. One goal of the AMMA field campaign was to improve the knowledge of the properties of the West African MCS. The goal of this study was to show that a MCS over a semi-arid region can create high concentration of ice nuclei in the upper troposphere. A joint investigation using both observations and models can serve to further understanding how aerosols can impact significantly the microphysics and the dynamics of an MCS in semi-arid region.

8. acknowledgments

The authors wish to thanks Jean-Pierre Chaboureau for providing the MSG brithness temperature pictures. MSG observations were obtained from Météo-France/Centre de Météorologie Spatiale through AMMASAT. Based on a French initiative, AMMA was built by an international scientific group and is currently funded by a large number of agencies, especially from France,

UK, US and Africa. It has been the beneficiary of a major financial contribution from the European Community's Sixth Framework Research Program. Detailed information on scientific coordination and funding is available on the AMMA international website http://www.amma-international.org.

References

Albrech, B., 1989. Aerosols, cloud microphysics, and fractional cloudiness. Science 245, 1227–1230.

Alfaro, S., Gomes, L., 2001. Modeling mineral aerosol production by wind erosion: Emission intensities and aerosol size distributions in source areas. J. Geophys. Res. 106 (D16), 18075–18084.

Andronache, C., 2003. Estimated variability of below-cloud aerosol removal by rainfall for observed aerosol size distributions. Atmos. Chem. Phys. 3, 131–143.

Barthe, C., Molini, G., Pinty, J., 2005. Description and first results of an explicit electrical scheme in a 3d cloud resolving model. Atmos. Res. 76, Issues 1-4, 95–113.

Bechtold, P., Bazile, E., Guichard, F., Mascart, P., Richard, E., 2001. A mass-flux convection scheme for regional and global models. Quart. J. Roy. Meteor. Soc. 127, 869–886.

Bougeault, P., Lacarrere, P., 1989. Parametrization of orography-induced turbulence in a meso-beta model. Mon. Wea. Rev. 117, 1872–1890.

BouKaram, D., Flamant, C., Knippertz, P., Reitebuch, O., Chong, M., Pelon, J., Dabas, A., 2008. Dust emissions over the sahel associated with the west african monsoon inter-tropical discontinuity region: a representative case study. Quart. J. Roy. Meteor. Soc. 134, 621–634.

Caniaux, G., Redelsperger, J., Lafore, J., 1994. A numerical study of the stratiform region of a fast-moving squall line. part i general description and water and heat budgets. J. Atmos. Sci. 51, 2046–2074.

Carrio, G., van den Heever, S., Cotton, W., 2007. Impacts of nucleating aerosol on anvil-cirrus clouds: A modeling study. Atm. Res. 84, 111–131.

Chaboureau, J., Pinty, J., 2006. Validation of a cirrus parameterization with meteosat second generation observations. Geophysical Res. Let. 33, doi:10.1029/2005GL024725.

Chin, M., Rood, R., Lin, S. J., Muller, J. F., Thompson, A., 2000. Atmospheric sulfur cycle simulated in the global model gocard: Model description and global properties. J. Geophys. Res. 105, 24,671–24,687.

Chomette, O., Legrand, M., Marticorena, M., 1999. Determination of the wind speed threshold for the emission of desert dust using satellite remote sensing in the thermal infrared. J. Geophys. Res. 104, 24,671–24,687.

Cohard, J., Pinty, J., 2000. A comprehensive two-moment warm microphysical bulk scheme . ii : 2d experiments with a non hysrostatic model. Quart. J. Roy. Meteor. Soc. 126, 1843–1859.

Crumeyrolle, S., Gomes, L., Tulet, P., Matsuki, A., Schwarzenboeck, A., Crahan-Kaku, K., 2008. Increase of the aerosol hygroscopicity by cloud

processing in a mesoscale convective system: a case study from the amma campaign. Atmos. Chem. Phys. 8 (23), 6907–6924.

DeMott, P., Sassen, K., Poellot, M., Baumgardner, D., Rogers, D., Brooks, S., Prenni, A., Kreidenweis, S., 2003. African dust aerosols as atmospheric ice nuclei. Geophysical Res. Let. 30 (14), 1732, doi:10.1029/2003GL017410.

Flamant, C., Chaboureau, J., Parker, D., Taylor, C., Cammas, J., Bock, O., Timouke, F., Pelon, J., 2007. Airborne observations of the impact of a convective system on the planetary boundary layer thermodynamics and aerosol distribution in the inter-tropical discontinuity region of the west african monsoon. Quart. J. Roy. Meteor. Soc. 133, 1175–1189.

Flamant, C., Knippertz, P., Parker, D., Chaboureau, J., Lavaysse, C., Agusti-Panareda, A., Kergoat, L., 2009. The impact of a mesoscale convective system cold pool on the northward propagation of the intertropical discontinuity over west africa. Quart. J. Roy. Meteor. Soc. 135, 139–159.

Gilmore, M., Straka, J. M., Rasmussen, E. N., 2004a. Precipitation and evolution sensitivity in simulated deep convective storms: Comparisons between liquid-only and simple ice and liquid phase microphysics. Mon. Wea. Rev. 132, 1897–1946.

Gilmore, M., Straka, J. M., Rasmussen, E. N., 2004b. Precipitation uncertainty due to variations in precipitation particle parameters within a simple microphysics scheme. Mon. Wea. Rev. 132, 2610–2627.

Ginoux, P., Chin, M., Tegen, I., Prospero, J., Holben, B., Dubovik, O., Lin,

S.-J., 2001. Sources and distributions of dust aerosols simulated with the gocart model. J. Geophys. Res. 106, 20255.

Grini, A., Tulet, P., Gomes, L., 2006. Dusty weather forecast using the mesonh atmospheric model. J. Geophys. Res. 111, doi:10.1029/2005JD007007.

Houghton, J., Ding, Y., Griggs, D. J., Noguer, M., van der Linden, P. J., Dai, X., Maskell, K., Johnson, C. A. (Eds.), 2001. IPCC 2001: *Climate Change 2001*. Cambridge University Press, Cambridge, England.

IPCC (Ed.), 2007. Climate change 2007: The scientific basis. Contribution of working group I to the Fourth Assessment Report of the Intergovernmental Panel on Climate Change. http://www.ipcc.ch/.

Jenkins, G., Pratt, A., Heymsfield, A., 2008. Possible linkages between saharan dust and tropical cyclone rain band invigoration in the eastern atlantic during namma-06. Geophysical Res. Let. 35, doi:10.1029/2008GL034072.

Kanji, Z., Abbatt, J., 2006. Laboratory studies of ice formation via deposition mode nucleation onto mineral dust and n-hexane soot samples. J. Geophys. Res. 111, doi:10.1029/2005JD006766.

Knippertz, P., Trentmann, J., Seifert, A., 2009. High-resolution simulations of convective cold pools over the northwestern sahara. J. Geophys. Res. 114 (D08110), doi:10.1029/2008JD011271.

Lafore, J., Stein, J., Asencio, N., Bougeault, P., Ducrocq, V., Duron, J., Fischer, C., Hereil, P., Mascart, P., Pinty, V. M. J., Redelsperger, J., Richard,

E., de Arellano, J. V.-G., 1998. The meso-nh atmospheric simulation system. part i: adiabatic formulation and control simulations. Ann. Geophys. 16, 90–109.

Levin, Z., Ganor, E., Gladstein, V., 1996. The effe1511-1523cts of desert particles coated with sulfate on rain formation in the eastern mediterranean. Journal of Applied Meteorology 35, 1511–1523.

Lin, Y., Farley, R., Orville, H., 1983. Bulk parameterization of the snow field in a cloud model. J. Climate Appl. Meteor. 22, 1065–1092.

Lohmann, U., Diehl, D., 2006. Sensitivity studies of the importance of dust ice nuclei for the indirect aerosol effect on stratiform mixed-phase clouds. J. Atmos. Sci. 63, 968–982.

Marsham, J., Parker, D., Grams, C., Haywood, J., 2008. Uplift of saharan dust south of the intertropical discontinuity. J. Geophys. Res. 113 (D21102), doi:10.1029/2008JD009844.

Marticorena, B., Bergametti, G., 1995. Modeling of the atmospheric dust cycle: 1. design of a soil derived dust emission scheme. J. Geophys. Res. 100, 16415–16429.

Masson, V., 2000. A physically-based scheme for the urban energy balance in atmospheric models. Boundary-Layer Meteorology 94, 357–397.

Min, Q., Li, R., Lin, B., Joseph, E., Wang, S., Hu, Y., Morris, V., Chang, F., 2009. Evidence of mineral dust altering cloud microphysics and precipitation. Atmos. Chem. Phys. 9, 3223–3231.

Nelson, J., 2001. Growth mechanisms to explain the primary and secondary habits of snow crystals. Phil. Mag. A 81, 10, 2337–2373.

Noilhan, J., Mahfouf, J., 1996. The isba land surface parameterization scheme. Global and Plan. Change 13, 145–159.

Pinty, J., Jabouille, P., 1998. A mixed-phase cloud parameterization for use in mesoscale non hydrostatic model: simulations of a squall line and of orographic precipitations. Conference of Cloud Physics Everett, WA, USA, 217–220.

Prenni, A., DeMott, P., Twohy, C., Poellot, M., Kreidenweis, S., Rogers, D., Brooks, S., Richardson, M., Heymsfield, A., 2007. Examinations of ice formation processes in florida cumuli using ice nuclei measurements of anvil ice crystal particle residues. J. Geophys. Res. 112 (D10221), doi:10.1029/2006JD007549.

Pruppacher, H., Klett, J., 2000. Microphysics of clouds and precipitation. Kluwer academic publishers.

Redelsperger, J., Thorncroft, D., A.Diedhiou, Lebel, T., Parker, D., Polcher, J., 2006. African monsoon multiplidisciplinary analysis: An international research project and field campaign. Bull. Am. Met. Soc. 87, 1739–1746.

Richardson, M., DeMott, P., Kreidenweis, S., Cziczo, D., Dunlea, E., Jimenez, J., Thomson, D., Ashbaugh, L., Borys, R., Westphal, D., Casuccio, G., Lersch, T., 2007. Measurements of heterogeneous ice nuclei in the western united states in springtime and their relation to aerosol characteristics. J. Geophys. Res. 112 (D02209), doi:10.1029/2006JD007500.

Sandu, I., Brenguier, J.-L., Geoffroy, O., Thouron, O., Masson, V., 2008. Aerosol impacts on the diurnal cycle of marine stratocumulus. J. Atmos. Sci. 65, 2705–2718, doi:10.1175/2008JAS2451.1.

Seinfeld, J., Pandis, S., 1997. Atmospheric Chemistry and Physics. Wiley interscience pub.

Slinn, W., 1983. Atmospheric sciences and power production 1979. Precipitation Scavenging, U.S. Department of Energy, Washington, D.C., chap. 11.

Suhre, K., Mari, C., Bates, T., Johnson, J., Rosset, R., Wang, Q., Bandy, A., Blake, D., Businger, S., Eisels, F., Huebert, B., Kok, G., Mauldin, R. I., Prévôt, A., Schillawski, R., Tanner, D., Thornton, D., 1998. Physicochemical modeling of the first aerosol characterization experiment (ace 1) lagrangian b, 1. a moving column approach. J. Geophys. Res. 103, 16433–16455.

Tegen, I., Lacis, A. A., 1996. Modeling of particle size distribution and its influence on the radiative properties of mineral dust aerosol. J. Geophys. Res. 101, 19237–19244.

Tost, H., Jockel, P., Kerkweg, A., Sander, R., Lelieveld, J., 2006. Technical note: A new comprehensive scavenging submodel for global atmospheric chemistry modelling. ACP 6, 565–574.

Tulet, P., Crassier, V., Cousin, F., Shure, K., Rosset, R., 2005. Orilam, a three moment lognormal aerosol scheme for mesoscale atmospheric model.

on-line coupling into the mesonh-c model and validation on the escompte campaign. J. Geophys. Res. 110, doi:10.1029/2004JD005716.

Tulet, P., Crassier, V., Solmon, F., Guedalia, D., Rosset, R., 2003. Description of the mesoscale nonhydrostatic chemistry model and application to a transboundary pollution episode between northern france and southern england. J. Geophys. Res. 108, D1, 4021.

Tulet, P., Grini, A., Griffin, R., Petitcol, S., 2006. Orilam-soa: A computationally efficient model for predicting secondary organic aerosols in 3d atmospheric models. J. Geophys. Res. 111, doi:10.1029/2006JD007152.

Twomey, S., 1959. The nuclei of natural cloud formation. part ii: The supersaturation in natural clouds and the variation of cloud droplet concentration. Pure Appl. Geophys. 43, 243–249.

van den Heever, S., Carrio, G., Cotton, W., Demott, P., Prenni, A., 2006. Impacts of nucleating aerosol on florida storms. part i: Mesoscale simulation. J. Atmos. Sci. 61, 1596–1609.

van den Heever, S., Cotton, W., 2004. The impact of hail size on simulated supercell storms. J. Atmos. Sci. 63, 1752–1775.

Zender, C., Bian, H., Newman, D., 2003. The mineral dust entrainment and deposition (dead) model: Description and global dust distribution. J. Geophys. Res. 108 (D14), 4416, http://dust.ess.uci.edu/dead/.

List of Figures

1 Brightness temperature from the MSG satellite (channel 10.8 μm, in K, color scale on the right), 1 July, 2006 at 18UTC (a), 2 July, 2006 at 00 UTC (c) and 2 July, 2006 at 02 UTC (e). Cloud top altitude (in km, color scale on the right) and instantaneous precipitation (isolines at 5, 25, 50, 75 $mmm.h^{-1}$) simulated by MesoNH on 1 July, 2006 at 17 UTC (b), 20 UTC (d) and 22 UTC (f). 33

2 Dust mass concentration ($\mu g.m^{-3}$) at the surface (colors, scale on the right) and 10 meter wind fields (arrows) simulated by MesoNH (SCAV) on 1 July, 2006 at 20 UTC. The solid line represents the vertical cross section of Figures 3, 4, 5 and 6. . 33

3 The vertical cross section of total condensate mixing ratio (shade in gkg^{-1}, scale on right) on 1 July at 20 UTC. Red isolines correspond to the mixing ratio of rain water (at 0.25, 0.75, 1.25, 2. 3. and 4. gkg^{-1}) and black isolines to the vertical velocity (dotted for subsidence at 1 and 0.5 ms^{-1} and solid lines for ascent motion at 1, 2, 5, 10, 15 and 20 ms^{-1}). At the bottom: the distance (in km) of the vertical cross section plotted on Figure 2 (the origin corresponds to the south west point). 33

4 The vertical cross section between 0 and 3000 m agl of simulation SCAV on 1 July at 20 UTC: (a) potential temperature (in K, color scale on the right), wind stream lines (solid lines with arrows) and kinetic turbulen energy (shaded, scale on the top); (b) dust mass concentration (in $\mu g.m^{-3}$, color scale on the right) and rain water mixing ratio (shaded, scale on the top). At the bottom: the distance (in km) of the vertical cross section plotted on Figure 2 (the origin corresponds to the south west point). 33

5 The vertical cross section of dust mass concentration on 1 July at 20 UTC of simulation NOSCAV ($\mu g.m^{-3}$, scale on right). At the bottom: the distance (in km) of the vertical cross section plotted on Figure 2 (the origin corresponds to the south west point). 33

6 The vertical cross section of the difference of dust mass concentration between NOSCAV and SCAV simulations ($\mu g.m^{-3}$, scale on right) on 1 July at 20 UTC. The dashed line corresponds to the vertical profile plotted in Figure 7. At the bottom: the distance (in km) of the vertical cross section plotted on Figure 2 (the origin corresponds to the south west point). . 34

7 A vertical profile in the convective region of the MCS simulated by MesoNH on 1 July, 2006 at 20 UTC on the cross-section indicated by the dashed line of Figure 6. Mass concentration (a) ($\mu g.m^{-3}$) and particles number concentration (b)(cm^{-3}) for modes at $R_g = 0.32\mu m$ (in green), $R_g = 1.73\mu m$ (in red) and $R_g = 4.33\mu m$ (in blue). The solid line represents the simulation SCAV and dashed line represents the simulation NOSCAV. 34

8 Dust number concentration (cm^{-3}, scale on right) of simulation SCAV, on July, 2 at 00 UTC at 16,000 m agl (a) and at 20,000 m agl (b). 34

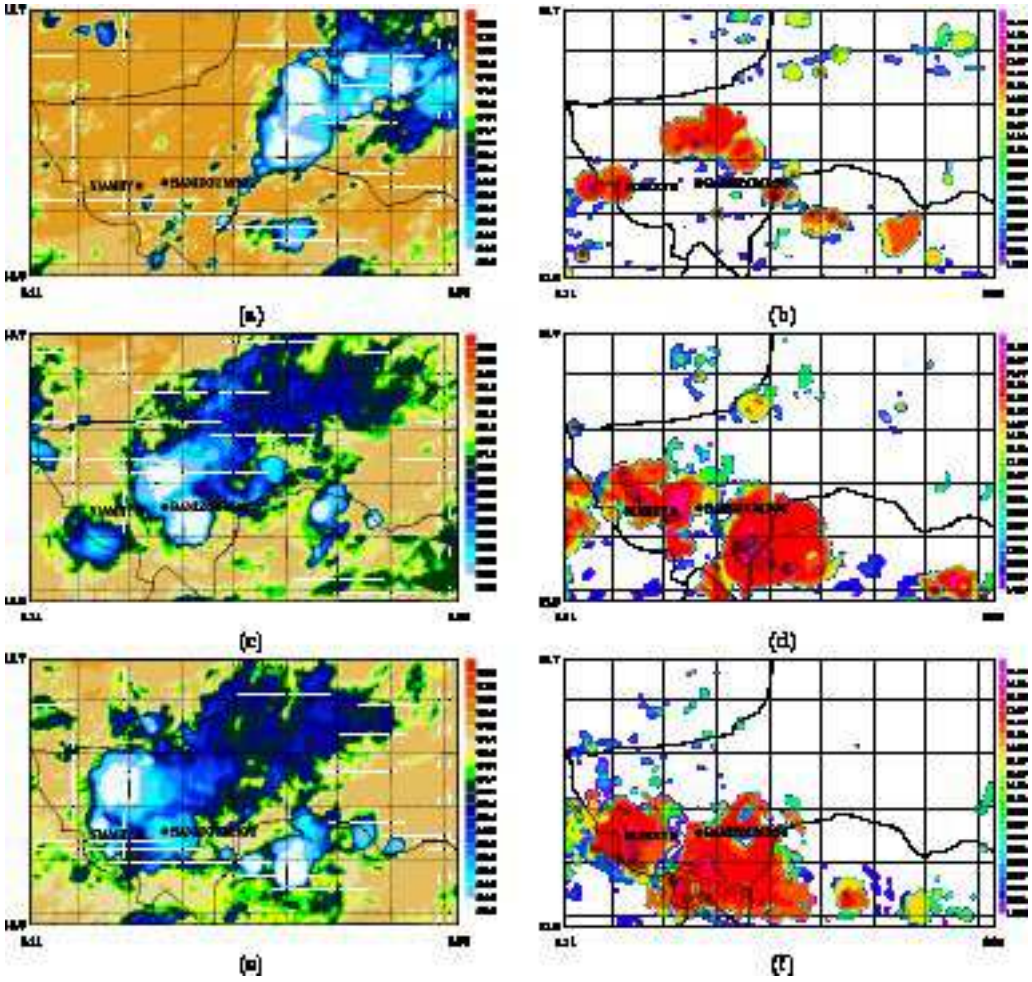

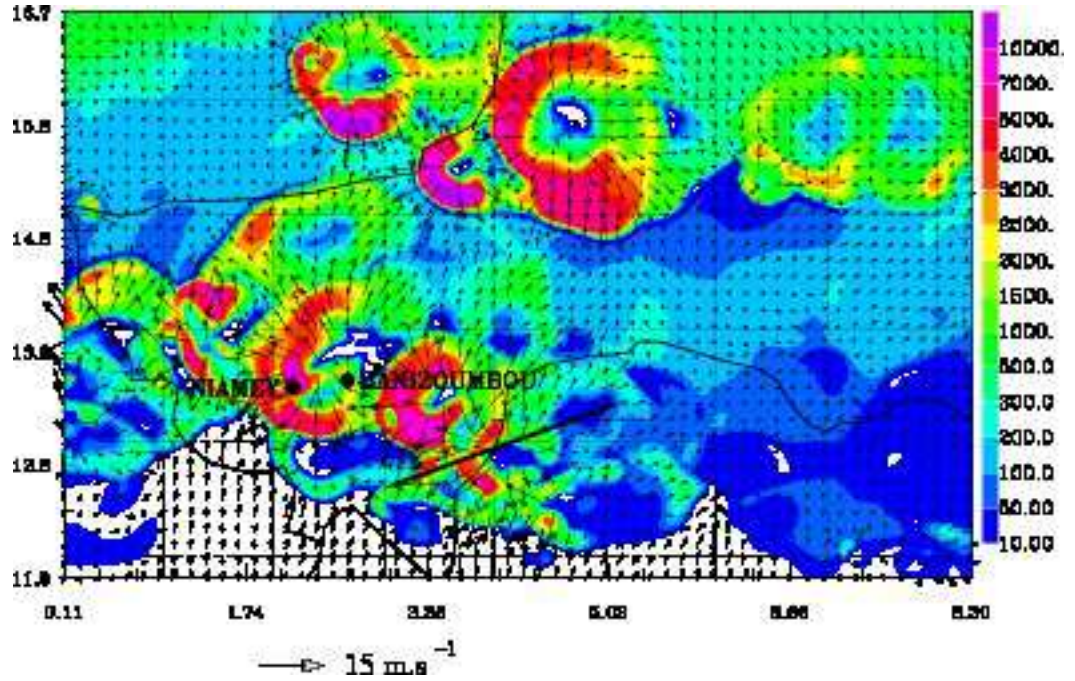
16.7
15.8
14.8
13.8
12.8
11.8
0.11
1.74
3.38
5.02
6.66
8.30
10000.
7000.
5000.
4000.
3000.
2500.
2000.
1500.
1000.
500.0
300.0
200.0
100.0
50.00
10.00
NIAMEY
15 m.s^{-1}

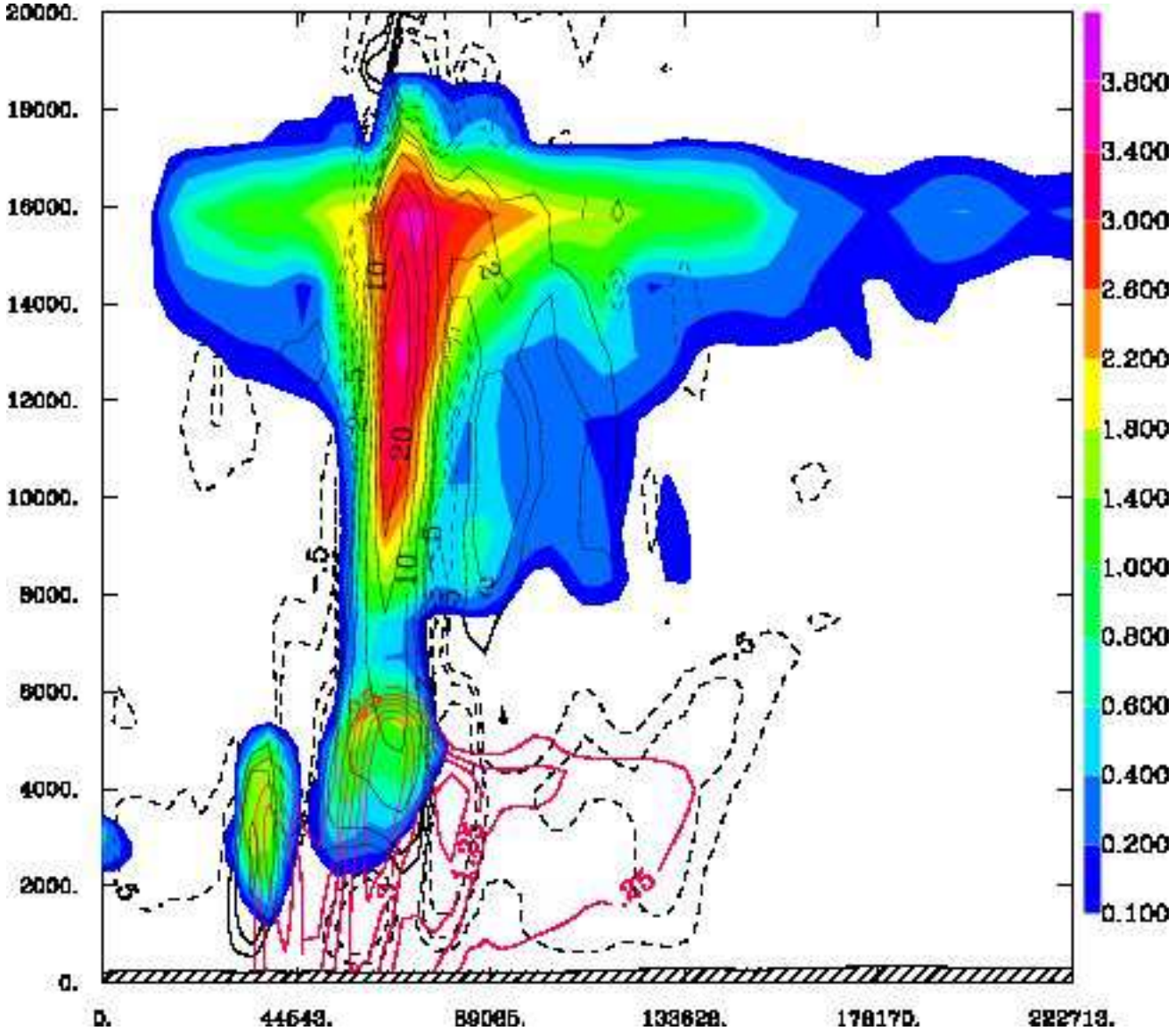
20000.
19000.
16000.
14000.
12000.
10000.
8000.
6000.
4000.
2000.
0.
0.
44643.
89065.
133628.
178170.
222713.
3.800
3.400
3.000
2.600
2.200
1.800
1.400
1.000
0.800
0.600
0.400
0.200
0.100

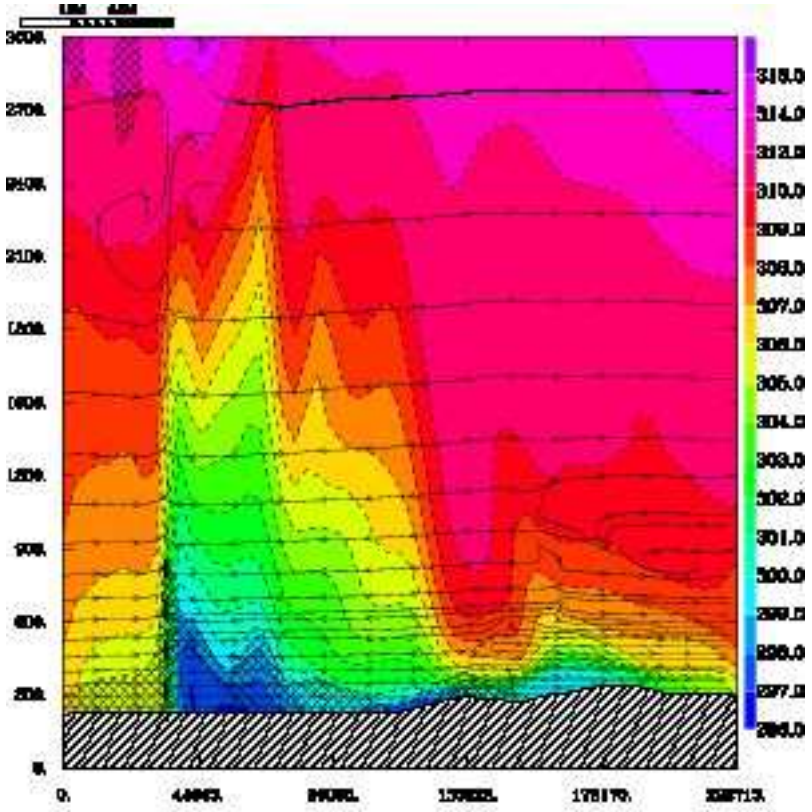

(a)

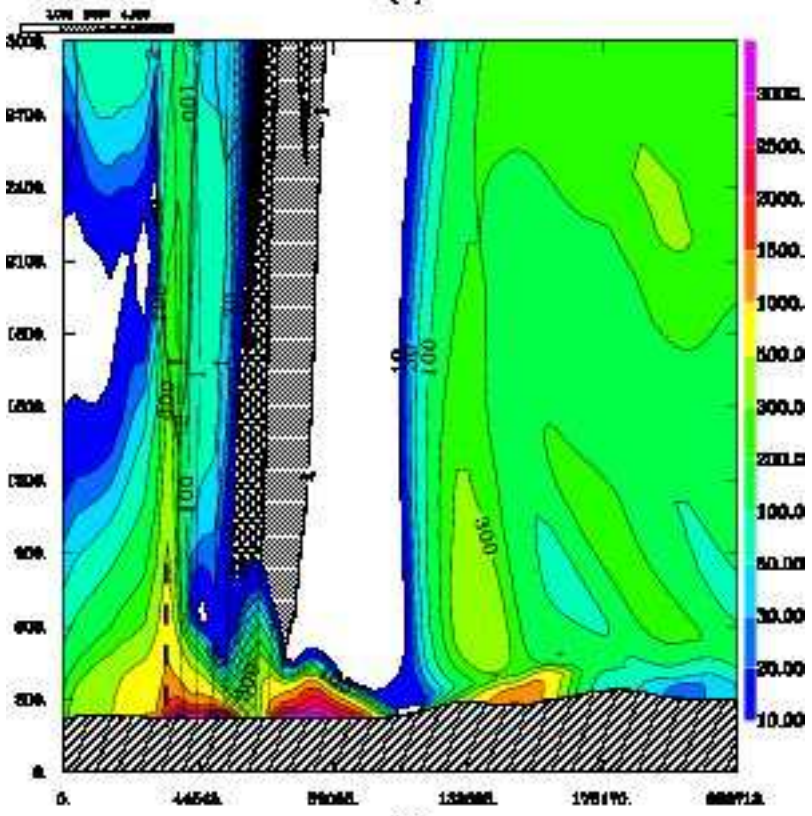

(b)

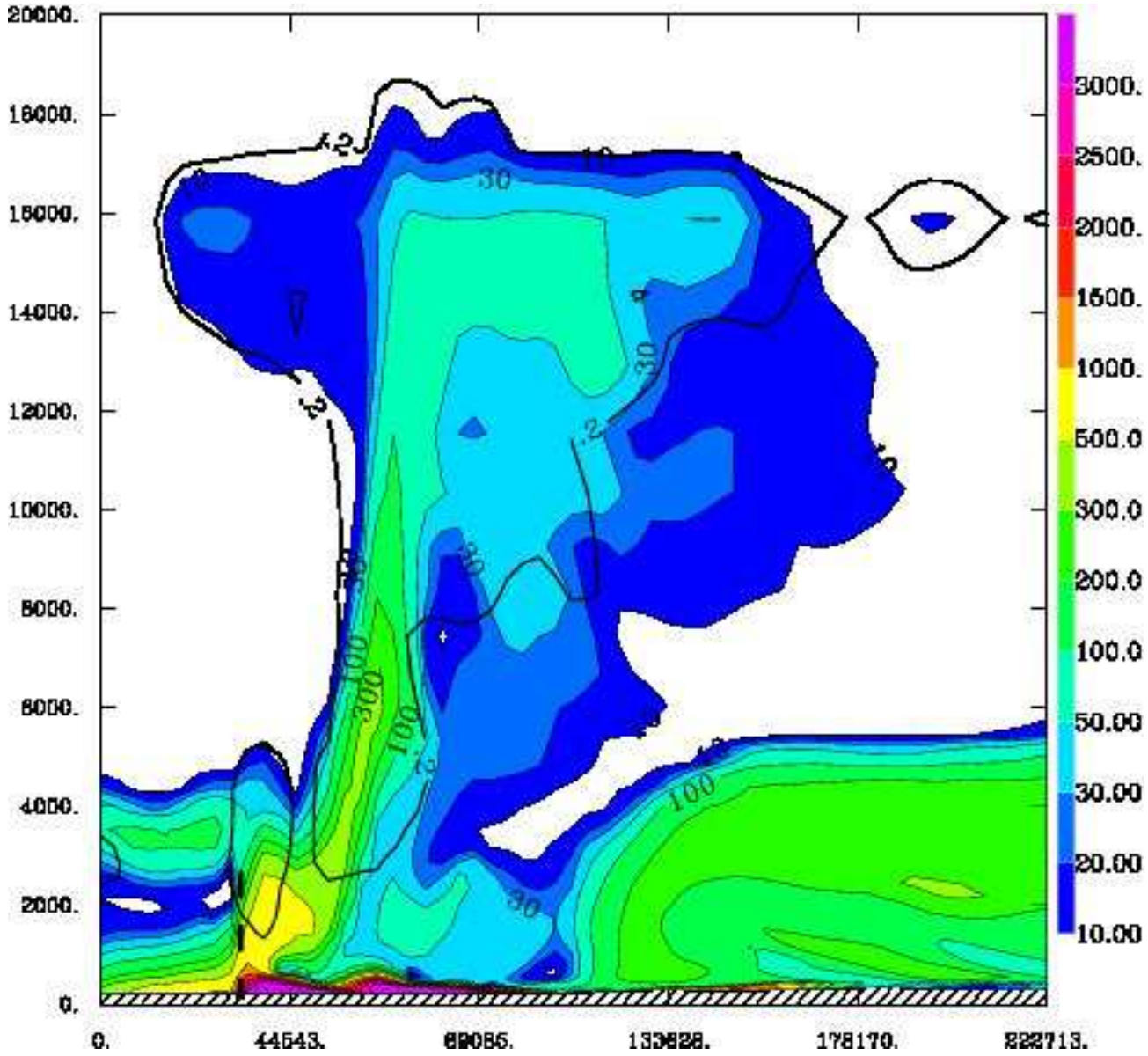
20000.
18000.
16000.
14000.
12000.
10000.
8000.
6000.
4000.
2000.
0.
0.
44543.
89086.
133628.
178170.
222713.
3000.
2500.
2000.
1500.
1000.
500.0
300.0
200.0
100.0
50.00
30.00
20.00
10.00

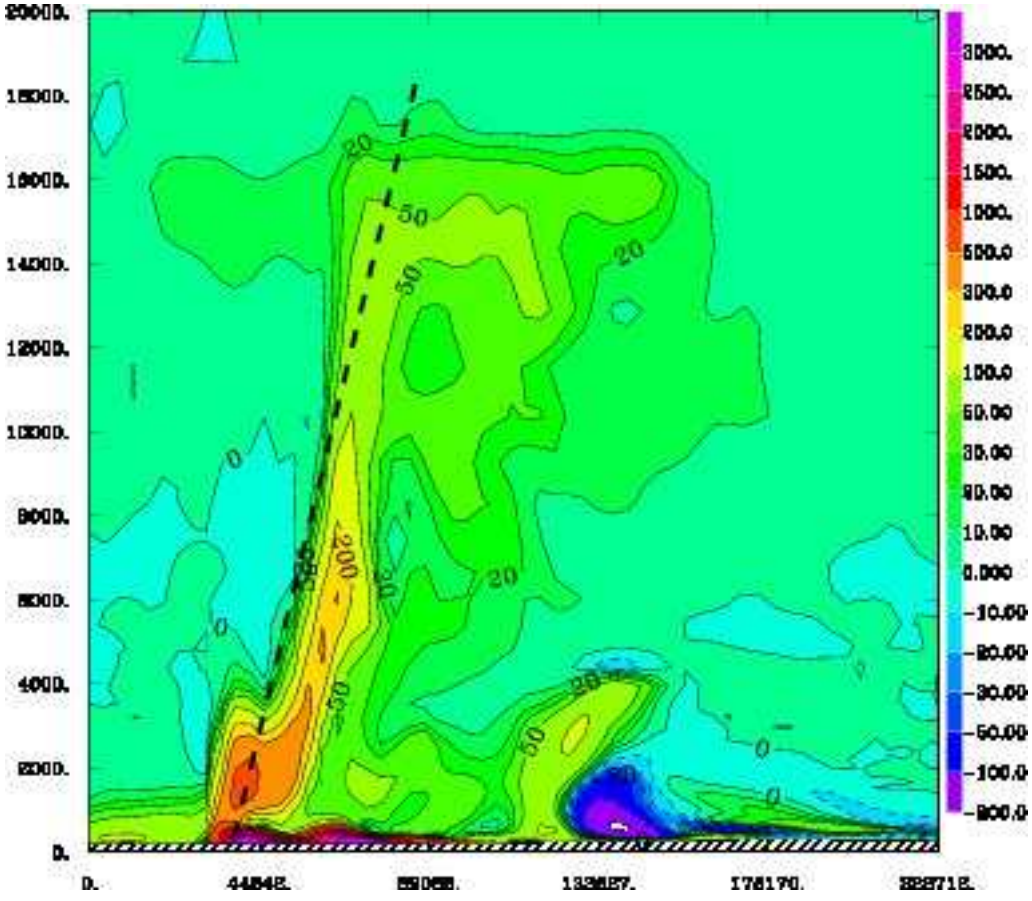
20000.
18000.
16000.
14000.
12000.
10000.
8000.
6000.
4000.
2000.
0.
0.
44848.
89088.
133627.
178170.
222712.
3000.
2500.
2000.
1500.
1000.
500.0
300.0
200.0
100.0
50.00
30.00
20.00
10.00
0.000
-10.00
-20.00
-30.00
-50.00
-100.0
-200.0
0
20
50
200

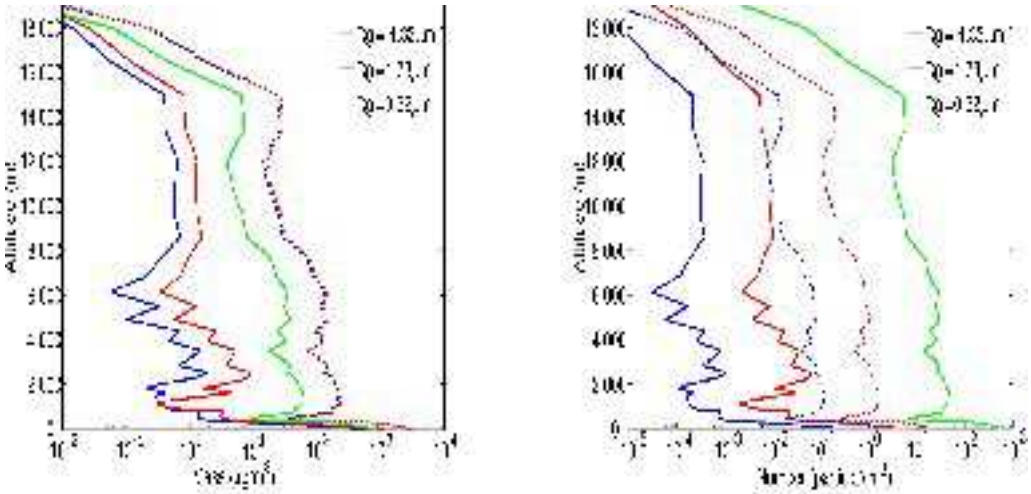
(a)
(b)

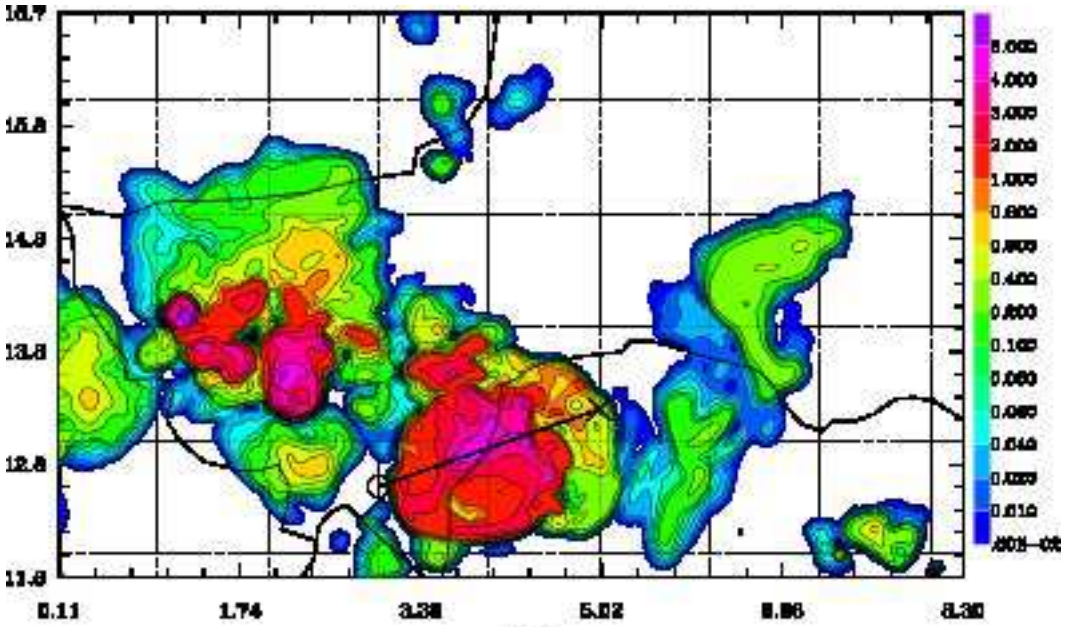
16.7
15.8
14.8
13.8
12.8
11.8
0.11
1.74
3.38
5.02
6.66
8.30

(a)

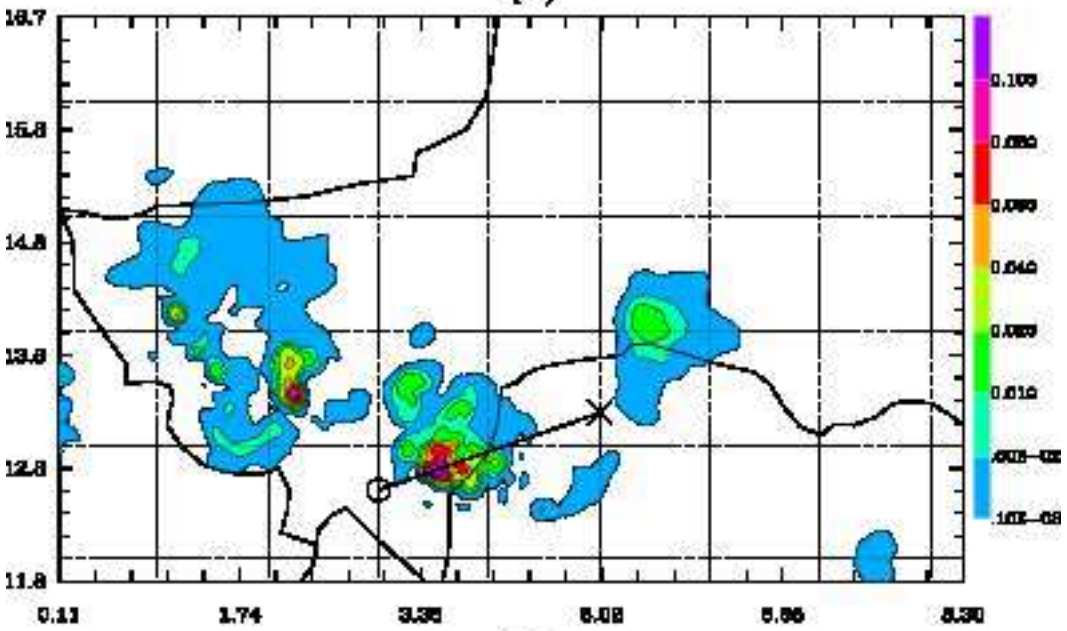
16.7
15.8
14.8
13.8
12.8
11.8
0.11
1.74
3.38
5.02
6.66
8.30

(b)